Experimental measurements of multiphoton enhanced air breakdown by a subthreshold intensity excimer laser

Jesse Way,[a] Jason Hummelt, and John Scharer
Department of Electrical and Computer Engineering, University of Wisconsin, Madison, Wisconsin 53706, USA

(Received 3 July 2009; accepted 14 September 2009; published online 23 October 2009)

This work presents density, spectroscopic temperature, and shockwave measurements of laser induced breakdown plasma in atmospheric air by subthreshold intensity (5.5×10^9 W/cm^2) 193 nm laser radiation. Using molecular spectroscopy and two-wavelength interferometry, it is shown that substantial ionization ($>10^{16}$ cm^{-3}) occurs that is not predicted by collisional cascade (CC) breakdown theory. While the focused laser irradiance is three orders of magnitude below the theoretical collisional breakdown threshold, the substantial photon energy at 193 nm (6.42 eV/photon) compared with the ionization potential of air (15.6 eV) significantly increases the probability of multiphoton ionization effects. By spectroscopically monitoring the intensity of the N_2^+ first negative system ($B\ ^2\Sigma_u^+ - X\ ^2\Sigma_g^+$) vibrational bandhead ($v'=0, v''=0$) at low pressure (20 Torr) where multiphoton effects are dominant, it is shown that two photon excitation, resonant enhanced multiphoton ionization is the primary mechanism for quantized ionization of N_2 to the $N_2^+(B\ ^2\Sigma_u^+)$ state. This multiphoton effect then serves to amplify the collisional breakdown process at higher pressures by electron seeding, thereby reducing the threshold intensity from that required via CC processes for breakdown and producing high density laser formed plasmas.
 [doi:10.1063/1.3245332]

I. INTRODUCTION

There has been a great deal of research on laser induced breakdown of gases, especially at visible and infrared wavelengths. Due to its fundamental nature, a large subset of this research has been devoted to studies of breakdown in air.[1–4] This paper reports experimental results of breakdown in air using sub-breakdown threshold intensity, 193 nm excimer laser radiation. Much of the theoretical basis of laser induced breakdown is based upon earlier work describing microwave breakdown.[5] The primary means by which breakdown occurs in the microwave, infrared, and optical wavelength regimes is a collisional cascade (CC) effect where initial electrons in the focal volume collide with neutrals after being excited by the incoming radiation. After many interactions with the electric field, the electron obtains an energy level greater than the ionization potential of the background gas and a subsequent collision can cause ionization of the neutral particle, thereby producing a secondary electron. This cascade or avalanche breakdown effect has been widely studied at microwave frequencies and an extensive review and discussion was written by Macdonald.[5] As mentioned above, the cascade breakdown effect is reliant upon having at least one free electron in the laser focal volume to start the process. A possible source of the initial electron(s) is through quantum multiphoton ionization (MPI), where a neutral particle absorbs enough laser photons within the excitation lifetime to increase its energy above the ionization potential.[1] An additional process involving quantum ion creation is resonant enhanced MPI (REMPI),[6,7] where a neutral particle is first energized to an excited state by the absorption of one or more photons and is then ionized from this state by receiving the required number of photons to overcome the ionization potential. MPI effects are strongly dependent on the photon energy of the laser and the probability of a MPI event in air at infrared wavelengths—where the photon energy is just a few percent or less of the ionization potential—is quite low.[8] However, at visible and especially ultraviolet (UV) wavelengths where the photon energy can be an appreciable fraction ($\sim1/3-1/2$) of the ionization potential, there is a much higher probability of MPI.

There has been recent interest and an increase in research on breakdown processes by UV lasers—particularly KrF (248 nm) lasers[9–11]—where multiphoton effects can play a significant role. We report results utilizing a 193 nm (6.42 eV/photon), ArF transition, excimer laser. In previous works[12,13] we investigated the density and temperature evolution of a 193 nm laser induced air plasma as well as the scaling of the breakdown threshold as compared with the microwave regime. For both of these experiments the plasma was created by a short focal length ($f=2$ cm) objective lens for which the focused irradiance ($1-10$ TW/cm^2) was greater than the collisional breakdown threshold of air.

In this paper we investigate 193 nm laser breakdown of air using a long ($f=18$ cm) focal length lens for which the plasma features are markedly different than the $f=2$ cm case. Rather than an intense spherical discharge, the longer focal length lens produces a more diffuse, cylindrical plasma with somewhat lower density and much cooler molecular temperatures. The long term objective is to utilize the longer focal length lens to produce a 193 nm seed plasma in air—without the use of a low ionization potential seed gas—for long pulse, large volume, radio frequency (rf) sustained air

[a]Electronic mail: jesse.m.way@gmail.com.

plasmas.[14] The focused irradiance input to the $f=18$ cm lens was varied in the range of 1–5 GW/cm^2, three orders of magnitude below the theoretical collisional breakdown threshold of 5 TW/cm^2 at standard temperature and pressure (STP).[15] In this regime we have observed substantial electron densities ($>10^{16}$/cc) in dry air at 760 Torr that we demonstrate is due in part to REMPI of N_2 as a source of seed electrons for CC breakdown. These seed electrons greatly enhance CC effects at low flux intensities[8] and allow significant ionization to occur at lower pressures (20 Torr) and air breakdown to occur at higher pressures (700–800 Torr).

II. THEORY

A. Classical breakdown theory

The collisional breakdown theory of gas by laser radiation is based on the microwave breakdown mechanism of cascade ionization where free electrons gain energy through electron-neutral inverse bremsstrahlung collisions.[1] Upon attaining an energy level greater than the ionization potential of the gas, the excited electron creates a secondary electron through impact ionization of a neutral. This process can generally be described by the reaction equation

$$e^- + M \rightarrow 2e^- + M^+, \tag{1}$$

where M is the neutral atom or molecule, M^+ is the resultant ion, and e^- is the electron. Some of the energy loss processes that must be overcome for electron cascade growth to occur include collisional excitation of molecular electronic states and vibrational and rotational degrees of freedom as well as electron losses due to attachment, recombination, and diffusion out of the focal volume. This process is described by the continuity equation as[15]

$$\frac{\delta n_e}{\delta t} = \nu_i n_e - \frac{D}{\Lambda^2} n_e - \nu_a n_e - \nu_r n_e^2, \tag{2}$$

where n_e is the electron density, ν_i is the ionization rate for electrons, ν_a is the electron attachment rate, ν_r the recombination rate, D the electron diffusion coefficient, and Λ the characteristic diffusion length. Assuming the collisional electron production rate is greater than the sum of the various loss rates, the electron density will grow exponentially in time during the laser pulse as[16]

$$n_e(t) = n_{eo} \exp(t/\tau_c), \tag{3}$$

where n_{eo} is the initial electron density and τ_c is the avalanche time constant defined as $\tau_c = 1/(\nu_i - \nu_a - \nu_r)$ when diffusion can be neglected, as is the case for our focal spot size.[15]

In general, the breakdown threshold can be determined by integrating Eq. (2) over time and requiring a certain amount of ionization by the end of the laser pulse. In calculating the collisionally induced breakdown threshold, we follow the approach of Smith and Meyerand, which assumes that electron diffusion and attachment are negligible, which is the usual case for high intensity laser ionization. The resulting breakdown intensity threshold can then be written as[15]

$$I_{\mathrm{BdCC}} = \left(\frac{8\times 10^2}{P t_p \lambda^2}\right)(1 + 4.5\times 10^{-6} P^2 \lambda^2)(1 + 2\times 10^8 t_p P), \tag{4}$$

where I_{BdCC} is in W/cm^2, λ is the laser wavelength in microns, P is the pressure in atmospheres, and t_p is the laser pulse length in seconds. At 760 Torr, the CC breakdown threshold of air at 193 nm is calculated as 5×10^{12} W/cm^2. When considering CC breakdown, it is often convenient to describe the radiation intensity in terms of an effective electric field that represents the effectiveness of the high frequency radiation in coupling its energy to electrons. This is done by scaling the electric field with the laser frequency and electron-neutral collision rate as[5,17]

$$E_{\mathrm{eff}} = E\left(1 + \frac{\omega^2}{\nu_c^2}\right)^{-1/2}, \tag{5}$$

where ω is the laser frequency, E is the electric field amplitude, and ν_c is the electron collision frequency. The electron-neutral collision frequency is defined as $\nu_c = \beta \times 10^9 P$, where β is an energy and gas dependent constant and P is the pressure in Torr. For air, a value of 5.3 is commonly used for β.[5,17] For 193 nm laser radiation and an air pressure of 760 Torr, $\omega \gg \nu_c$ and the effective field can be written as $E_{\mathrm{eff}} = E(\nu_c/\omega)$.

B. Multiphoton ionization

At UV laser wavelengths, there exists a high probability of multiphoton ionization of neutrals. In this quantum process, an atom or molecule absorbs enough laser photons within the excitation lifetime to become ionized. The excitation lifetime is given by the uncertainty principle as $\tau = h/\varepsilon_i$ ($\tau = 6.5\times 10^{-16}$ s at 193 nm), where ε_i is the laser photon energy[18] and h is the Planck constant. Multiphoton ionization can most simply be described by the reaction equation

$$M + mh\nu \rightarrow M^+ + e^-, \tag{6}$$

where m is an integer number of photons and ν is the laser frequency. To achieve ionization, the number of photons m must exceed the integer portion of $(\varphi_i/h\nu + 1)$, where φ_i is the ionization potential of the neutral in joules. The probability that a neutral will be ionized by MPI is proportional to the probability of the absorption of m photons and scales as

$$\omega_o \propto I^m, \tag{7}$$

where ω_o is the probability of ionization and I is the intensity of the laser beam. To theoretically determine MPI rates Keldysh[19] developed a nonperturbative approach based on the problem of a hydrogen atom in a strong radiation field. In the limit that the optical frequency is much greater than the frequency of an electron penetrating the potential barrier, the ionization rate can be written as[19]

$$\omega_o = A\omega m^{3/2}\left(\frac{e^2E^2}{8m_e\omega^2\varphi_i}\right)^m, \tag{8}$$

where ω is the optical frequency, m_e is the electron mass, and A is a factor of order unity. If a mean balanced ionization

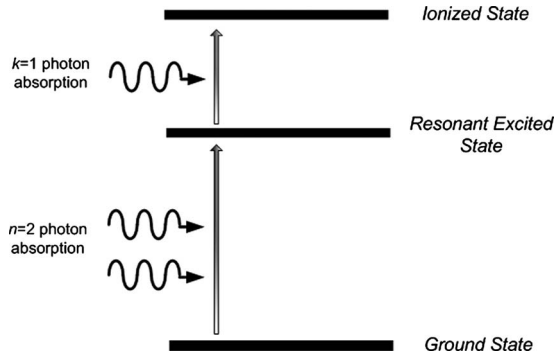

FIG. 1. Illustration of 2+1 REMPI. Absorption of $n=2$ photons raises the molecule to an excited state followed by the absorption of $k=1$ photon for ionization.

potential of 15.6 eV is used for air (O_2 and N_2),[5,17] Eq. (8) predicts a rate of 150 s^{-1} for 193 nm laser radiation at a flux intensity of 5.5×10^9 W/cm^2. In air at 760 Torr with a typical laser focal volume of 10^{-5} cm^3, this corresponds to an electron density of 10^{11} cm^{-3} with 20 ns laser pulses. We find that this result is in agreement with another theoretical MPI model developed by Tozer[18] that calculates the ionization rate based on the probability of a collision between an atom and a photon and can be written as

$$\omega_o = \frac{(1/\tau)(\psi\sigma\tau)^m}{m!}, \tag{9}$$

where ψ is the photon flux, σ is the photon cross section, τ is the quantum lifetime, and m is the integer number of photons for ionization.

C. Resonant enhanced multiphoton ionization

Another form of quantum ionization is REMPI. If an atom or molecule has a resonant excited state very near or at an integer multiple of the photon energy, there exists the possibility of REMPI. This is particularly true for molecular gases such as air because small energy differences between resonant state energy levels and quantized photon energy levels can be satisfied by the substantial molecular vibrational degrees of freedom.[19] In an $n+k$ REMPI process, an atom or molecule absorbs n photons to excite it to a resonant state from which it absorbs an additional k photon(s) to become ionized. This is graphically illustrated in Fig. 1 for a 2+1 REMPI process. This effect can lead to greatly enhanced multiphoton ionization rates[8] by effectively lowering the order of the process from m, the number of photons required for direct ionization, to n, the number of photons required for excitation to a resonant state ($n<m$). For an $n+k$ REMPI process the rate equations are given as[6]

$$\frac{dX}{dt} = -\alpha X + (\alpha+\gamma)A, \tag{10}$$

$$\frac{dA}{dt} = \alpha X - (\alpha+\beta+\delta+\gamma)A, \tag{11}$$

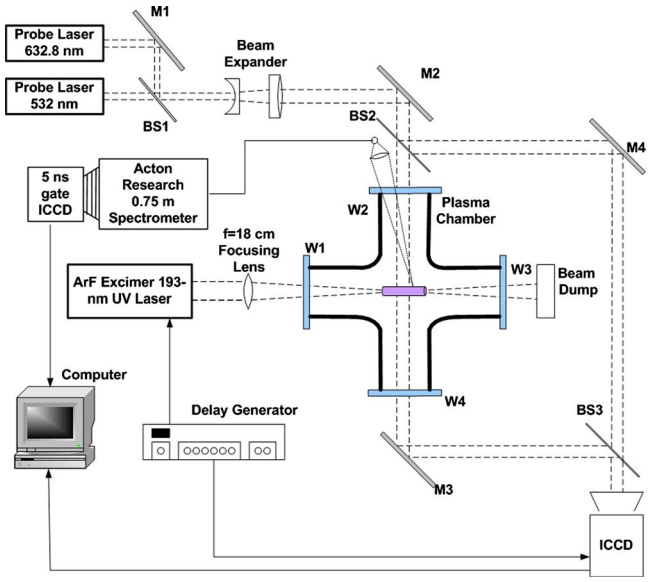

FIG. 2. (Color online) Schematic representation of the 193 nm laser induced plasma experimental system including a two-wavelength interferometer, spectrometer, and shadowgraphy optical diagnostic equipment. BS—beamsplitter, M—mirror, and W—window.

$$\frac{dC}{dt} = \beta A, \tag{12}$$

where X, A, and C are the number density of molecules at the ground, resonant, and ionization states, respectively, α is the n photon stimulated absorption constant, β is the k photon ionization constant, γ is the fluorescence rate, and δ is the radiationless transition rate to a species that does not ionize. The constants α and β are defined as $\alpha=\sigma_n I^n$ and $\beta=\sigma_k I^k$, where σ_n and σ_k are the n and k photon cross sections, respectively, and I is the laser flux. From Eqs. (10)–(12) the ionization rate can be written as[6]

$$\omega_o = \frac{X\sigma_n\sigma_k I^{n+k}}{\sigma_k I^k + \delta + \gamma}. \tag{13}$$

In the limit of moderate laser intensities such as those encountered here, the solution to the above rate equations is of the form $\sim\sigma_n I^n$ with the result that the ionization probability is proportional to the resonant process order of nonlinearity n and not the sum $n+k$.

III. EXPERIMENTS

A. Laser focused plasma system

Shown in Fig. 2 is a diagram of our experimental setup including the laser focused plasma system and optical diagnostic equipment. The basic experimental layout has been described elsewhere[12] but a brief description is included here for completeness. The heart of the system is a Lumonics Pulsemaster PM-842 excimer laser operating in the ArF mode producing a uniform intensity, rectangular (2.8×1 cm^2) output beam at 193 nm wavelength. The maximum radiated energy was 260 mJ over 20 ns providing a maximum output power of 13 MW. The output beam was focused into a vacuum chamber through a coated fused silica window by an $f=18$ cm planoconvex lens. The focusing lens used

was also made of fused silica and was antireflection coated on both surfaces to provide 97.7% transmission at 193 nm. Assuming a cylindrical focal volume, the radius and axial length can be approximated by:[17] $r_o=f(\alpha/2)$ and $l_o=[\sqrt{(2)}-1](\alpha/d)f^2$, where α is the input beam divergence, d is the diameter of the unfocused beam, and f is the lens focal length. For our laser with $\alpha=3$ mrad, $d=1$ cm, and an $f=18$ cm lens, the radius and axial length are $r_o=270$ μm and $l_o=4$ mm. For plasma diagnostics the experimental setup included a two-wavelength interferometer, a high resolution spectrometer with light collection optics, and a shadowgraph imaging system.

B. Two-wavelength interferometer

To measure the plasma density we utilized a two-wavelength interferometer in a Mach–Zehnder configuration. The measurement arm of the interferometer was passed through the plasma in the vacuum chamber after which it was recombined with the reference arm and captured by an Andor Istar DH-734 fast gating (5 ns) intensified charge coupled device (ICCD). Initially, one of the mirrors of the interferometer was slightly tilted to produce a periodic fringe pattern at the ICCD. This image was then used as a reference and could be subtracted from subsequent fringe patterns produced by the plasma to determine the induced phase shift. Great care was taken to align the interferometer to have perfectly vertical reference fringes, which is necessary for unambiguous determination of the phase perturbation. For probe beams, a 532 nm (green) solid state and a 632.8 nm (red) helium-neon laser were used, both with power levels $\leq$10 mW. The probe beams were combined with a mirror and 50/50 beamsplitter and expanded to a diameter of 2 cm before entering the interferometer. Because of the contribution of neutrals to the plasma refractive index, a two-wavelength technique was necessary to separate the neutral and electron phase shifts in the plasma.[20] The phase shift in the probe beam due to the electron component in the plasma can be written as[21]

$$\varphi_e = \frac{e^2\lambda_p}{4\pi m_e \varepsilon_o c^2}\int_0^L n_e(r)dr = r_e\lambda_p\int_0^L n_e(r)dr, \tag{14}$$

where e is the electron charge, λ_p is the probe laser wavelength, r_e is the classical electron radius (2.818×10^{-13} cm), and $n_e(r)$ is the electron density profile. Assuming a mean path length L of the probe beam through the plasma in the radial direction, the electron contribution to the total phase shift can be simplified to a line integrated quantity as

$$\varphi_e = -r_e\lambda_p n_e L, \tag{15}$$

where the phase shift is negative because the refractive index is less than one. Similarly, the line integrated phase shift caused by the neutrals can be written as[21]

$$\varphi_n = \frac{2\pi}{\lambda_p}\frac{\beta}{n_{\text{atm}}}nL, \tag{16}$$

where n_{atm} is the atmospheric density at standard pressure and temperature, n is the neutral density, and β is the Gladstone–Dale constant multiplied by the density of the gas mixture.[22] In general, the total phase shift induced by the plasma is a sum of the contributions of the separate plasma components. Using two probe laser beams and combining Eqs. (2) and (3), the line integrated electron density is then expressed as[21]

$$n_e = \frac{1}{r_e L}\frac{\varphi_r\lambda_r - \varphi_g\lambda_g}{\lambda_g^2 - \lambda_r^2}, \tag{17}$$

where φ_r and λ_r are the red phase shift and wavelength (632.8 nm) and φ_g and λ_g are the green phase shift and wavelength (532 nm).

To extract spatial phase information from the interferometer fringe data, a software package called IDEA was used.[23] IDEA is an acronym for interferometric data evaluation algorithm and was developed at Technical University Graz. IDEA performs a two-dimensional Fourier transform on the interference fringes to determine local phase profiles. Using the interference equation, the spatial intensity profile of the fringe pattern with carrier frequency in the x-direction can be written in complex notation as[23]

$$i(x,y) = i_o(x,y) + c(x,y)e^{2\pi\nu_o x} + c^*(x,y)e^{-2\pi\nu_o x}, \tag{18}$$

where $i_o(x,y)$ is the background intensity distribution, υ_o is the carrier fringe frequency, and $c(x,y)$ is a function dependent on the induced phase distribution $\varphi(x,y)$. The asterisk superscript denotes the complex conjugate. By taking the Fourier transform of Eq. (18) and filtering out all frequencies which are not equal to the carrier frequency, the carrier frequency data can be removed with a shift back to the origin. A subsequent transformation back to the spatial domain yields the complex amplitude $c(x,y)$ from which the phase distribution can be obtained from[23]

$$\phi(x,y) = \arctan\left(\frac{\text{Im}\{c(x,y)\}}{\text{Re}\{c(x,y)\}}\right), \tag{19}$$

where Im { } and Re { } denote the imaginary and real parts of $c(x,y)$, respectively. Using this method, the phase shift induced within the plasma can be determined with an accuracy of up to $2\pi/100$ rad.[23] Shown in Fig. 3 are examples of an interferogram with the plasma in place, and the resultant phase distribution calculated using IDEA.

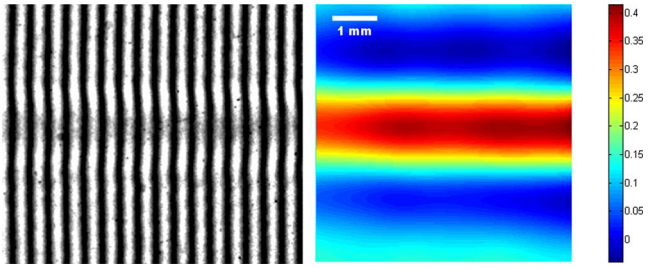

FIG. 3. (Color online) Sample interferogram with plasma in the measurement arm (left) and the resultant phase distribution in radians calculated using IDEA fringe analysis software (right).

C. Optical emission spectroscopy

Our experimental setup also included an optical emission spectroscopy diagnostic with which we measured the

plasma molecular temperatures as well as multiphoton ionization phenomena. At breakdown, the plasma emission was captured by a 1-in.-diameter fused silica objective lens and collimator system and then coupled into a broadband (200–800 nm) fiber optic cable. The fiber output was then coupled to a 0.75 m focal length Acton SpectraPro 2750 spectrometer configured with a 2400 g/mm holographic grating providing a resolution of 0.01 nm with a 100 μm slit width. The output of the spectrometer was then captured by an ICCD capable of gating times as short as 5 ns.

Using the spectrometer in conjunction with SPECAIR, a spectroscopic software modeling package developed by Laux *et al.*,[24] the vibrational and rotational temperatures of the plasma were measured by monitoring the N_2^+ first negative ($B\,^2\Sigma_u^+ - X\,^2\Sigma_g^+$) band system emission.[14] SPECAIR determines the populations of radiative states in air based on user defined electronic, vibrational, rotational, and translational temperature values. By fitting the software generated plots with the experimental spectral data, we were able to determine the plasma vibrational and rotational temperatures.

In addition to plasma temperature measurements, the spectrometer was also used to measure multiphoton ionization effects. The formal intensity law describes the $\sim I^m$ laser intensity dependence of multiphoton processes such as excitation and ionization.[25] Accordingly, the slope of a log-log plot of ion signal versus laser intensity yields the order of nonlinearity m of the rate-limiting quantum ion creation process. By measuring the peak intensity of the N_2^+ first negative ($v'=0, v''=0$) bandhead at low pressure where collisional effects are negligible one can measure the order of the photon process m.

D. Shadowgraphy

As a final diagnostic tool, the experimental setup included a laser shadowgraph system with which the spatial and temporal evolution of the plasma and associated shockwave were observed.[12,22,26] The measurements were made by passing a 532 nm probe beam through the laser formed plasma, perpendicular to the direction of propagation of the 193 nm pulse. The probe beam was expanded to a diameter of 2 cm before passing through the plasma, after which the resultant image was captured by a fast gating ICCD with a 1:1 aspect ratio. The shadowgraph technique is useful for visualizing perturbations in the refractive index of a material such as is found in shockwaves and plasmas. As light rays pass through a material under investigation they are refracted out of their original path. If the second spatial derivative of the refractive index of the material $\partial^2 n/\partial x^2$ is nonuniform over the path length, rays passing through a region with greater $\partial^2 n/\partial x^2$ will experience greater refraction thereby producing a shadow in the image corresponding to that region. Shown in Fig. 4 is a series of six shadowgrams taken at several times during the plasma decay. In addition to defining the cylindrical boundaries of the plasma, the shadowgrams were also useful for tracking the position of the shockwave as it propagated outward. For these images $t=0$ was immediately at the end of the 20 ns UV laser pulse.

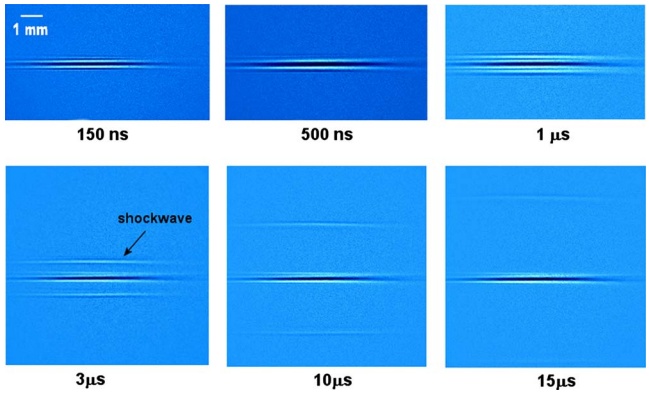

FIG. 4. (Color online) Shadowgrams of the subthreshold intensity, 193 nm, laser induced plasma and associated shockwave.

IV. MEASUREMENTS AND RESULTS

A. Plasma density

In air breakdown experiments the criterion that is used to assess whether or not breakdown has occurred is the presence of a visible bluish-white flash in the laser focal volume.[16,17] It has also been experimentally determined that this flash corresponds to approximately 10^{13} avalanche electrons.[16] Given our laser focal volume of 9×10^{-4} cm^3, this corresponds to an electron density of 1×10^{16} cm^{-3}. While the focused irradiance was three orders of magnitude below the classically predicted collisional breakdown threshold of air at 760 Torr, a bright discharge from the focal volume was noted, as is shown in Fig. 5. To verify substantial levels of ionization in the sub-breakdown threshold laser induced plasma, two-wavelength interferometry in conjunction with IDEA image processing software were used to measure the electron density. Due to the small phase shifts involved, the use of Fourier transform techniques applied by IDEA was essential to accurately measure the induced phase shift. Figure 6 shows the electron density decay in air at 760 Torr from 500 ns to 2 μs after the laser pulse. The measured laser energy was 260 mJ corresponding to a focused irradiance of 5.5×10^9 W/cm^2 after accounting for losses in the focusing lens and chamber window. An exponential fit indicates a density decay lifetime of 1 μs. At times earlier than 500 ns the small size and rapid expansion of the plasma make the interferogram fringe analysis technique unreliable and after 2 μs the electron density is reduced below the minimum sensitivity level of the instrument. The minimum measurable electron concentration for the interferometer can be written as[20]

$$n_e(\min) = \frac{\delta c^2}{0.404\times10^8 \lambda L}, \tag{20}$$

where δ is the minimum measurable fractional fringe spacing, c is the speed of light in cm/s, and λ and L are the laser

FIG. 5. (Color online) 193 nm laser induced plasma image captured with 75 mm focal length lens.

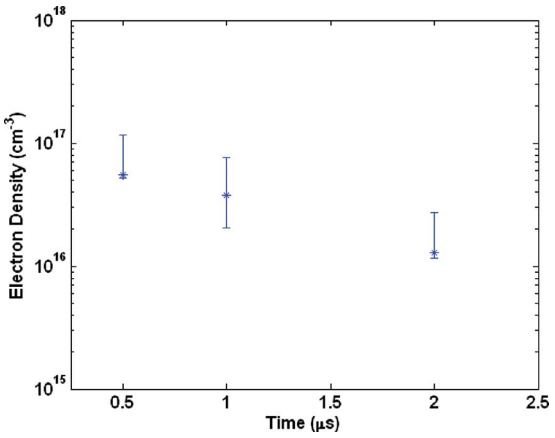

FIG. 6. (Color online) Plasma line averaged electron density in dry air at 760 Torr with a laser pulse energy of 260 mJ corresponding to a focused irradiance of 5.5×10^9 W/cm^2.

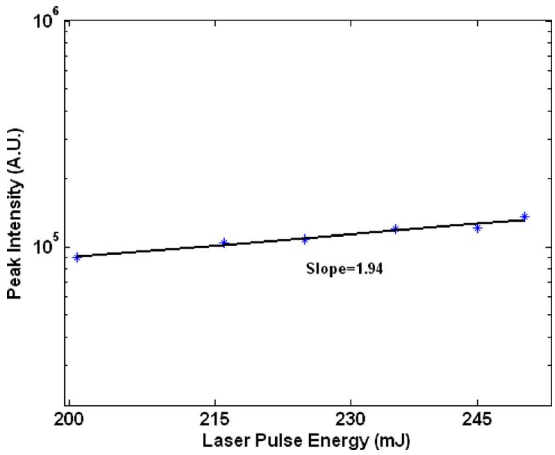

FIG. 7. (Color online) Log-log plot of the peak intensity of the N_2^+ first negative ($v'=0, v=0''$) bandhead at 391.4 nm as function of laser energy in dry air at 20 Torr. Slope indicates 2+1 REMPI of N_2.

wavelength and plasma path length in centimeters. Using IDEA, the minimum measurable phase shift is $2\pi/100$ (0.063) rad, which in our system corresponds to $\delta=1/100^{\text{th}}$ of a fringe spacing. Inserting this into Eq. (20) along with the red laser wavelength of 632.8 nm and plasma path length of 0.1 cm determined from shadowgraphic measurements, the minimum measurable electron density is 3.5×10^{16} cm^{-3}. This corresponds well with the last measured data point at 2 μs after which the interference phase shift was too small to measure accurately.

B. REMPI

In deriving CC breakdown models, the assumption of an initial electron in the focal volume is essential to start the avalanche process. In laser induced breakdown of air, it is often suggested that multiphoton effects play a role in the creation of initial electrons,[8] particularly at UV wavelengths. It has also been shown that multiphoton ionization can act as a seed for CC ionization in gas mixtures effectively amplifying the collisional process.[27] Here multiphoton effects in the laser induced plasma were investigated by spectroscopically monitoring the peak intensity of the N_2^+ first negative system ($v=0', v''=0$) bandhead at 391.4 nm as a function of laser energy. The measurements were carried out at 20 Torr where multiphoton effects are dominant over collisional effects.[16] By plotting the amplitude of the bandhead versus laser irradiance on a log-log plot, one obtains the order of the quantum multiphoton effect.[11,28,29] Figure 7 shows the intensity of the 391.4 nm bandhead over a range of laser pulse energies at 20 Torr. A least-squares fit to the data give a slope of 1.94 (97% correlation coefficient) indicating a two-photon excitation as the rate limiting process. This suggests that resonant 2+1 ionization is a dominant mechanism of quantum ionization of N_2 to the N_2^+ ($B\ ^2\Sigma_u^+$) state. Experimental investigation of pure nitrogen at higher pressures (~550 Torr) where collisional effects are more significant was published in a Letter by Gutherie *et al.*[11] In this brief note they obtained a peak bandhead slope of 1.6 which they attributed to the 2+1 REMPI of N_2 and suggested the $a\ ^1\Pi_g(v'=26)$ excited state as a likely candidate for the two-photon resonant level with 193 nm radiation. While our REMPI experiments were done in low pressure (20 Torr) dry air as opposed to nitrogen, it is anticipated that the $a\ ^1\Pi_g(v'=26)$ state of N_2 is also a likely candidate for the two-photon resonant level excitation. This is due to the fact that the quantum excitation mechanism of N_2 at low pressure is not dependent on the constituent components of the background gas mixture. The effect of pressure on the 391.4 nm bandhead intensity was also investigated while maintaining constant laser irradiance. Figure 8 shows the peak amplitude of the bandhead as the pressure was varied from 20 to 800 Torr in dry air with a laser pulse energy of 260 mJ. As the pressure was increased from 20 Torr the bandhead intensity increased linearly up to 500 Torr indicating increasing ion yields at higher pressure. After 500 Torr the bandhead intensity began to level off and then flattened up to 800 Torr indicating that the collisional quenching rate of the excited nitrogen states was of the same order or larger than the spontaneous radiative decay rate of the $B\ ^2\Sigma_u^+$ state[30] in this pressure range.

C. Spectroscopic temperature

Optical emission spectroscopy was also used to measure the rotational and vibrational temperatures of the plasma in

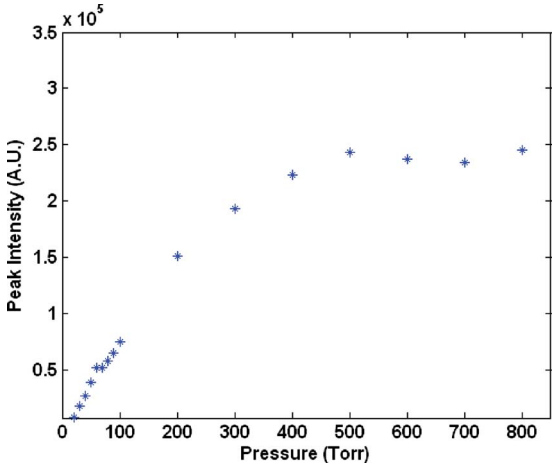

FIG. 8. (Color online) Pressure scaling of the N_2^+ first negative ($v'=0, v=0''$) bandhead at 391.4 nm from 20 to 800 Torr in dry air with 260 mJ laser pulses.

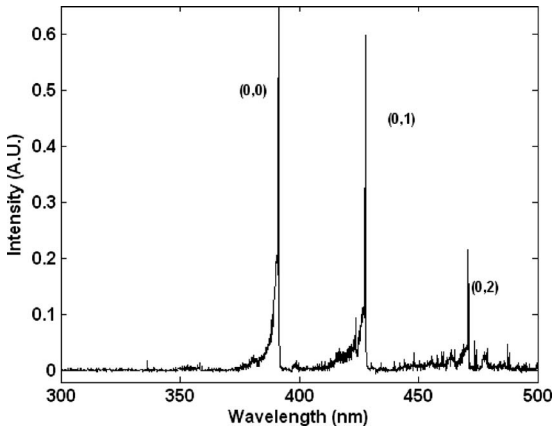

FIG. 9. Broadband emission spectra in dry air at 760 Torr identified as the N_2^+ first negative band system. The dominant peaks belong to the $(v'=0, v=0'')$, $(v'=0, v=1'')$, and $(v'=0, v=2'')$ vibrational bandheads.

dry air at 760 Torr. Shown in Fig. 9 is a broadband spectroscopic measurement from 300 to 500 nm, which indicates that the N_2^+ first negative system was the primary source of emission in this region.[31] The dominant peaks on the figure are the $(v'=0, v''=0)$ vibrational bandhead at 391.4 nm, the $(v'=0, v''=1)$ bandhead at 427.5 nm and the $(v'=0, v''=2)$ bandhead at 470.6 nm. To determine the temperatures, the measured spectra were fit with SPECAIR simulated profiles which are varied via user input temperature values. For comparison this was done for two regions of the spectrum; the $(v'=0, v''=0)$ portion around 391.4 nm and the $(v'=0, v''=1)$ portion around 427.5 nm, both of which showed similar results. Figure 10 illustrates the measured spectra from 423 to 428 nm, which includes the $(v'=0, v''=1)$ and $(v'=1, v''=2)$ vibrational bandhead peaks. The measured results were fitted with the SPECAIR simulation results with very good agreement. To improve signal strength, the measured spectra were obtained with background subtracted averages of 2000 laser shots, each with a 5 ns integration time. Because the lifetime of the N_2^+ emission can be as short as 1 ns at high pressure,[11] the signal integration time began immediately after the end of the UV laser pulse. The best-fit simulation results for both portions of the spectrum yield a rotational

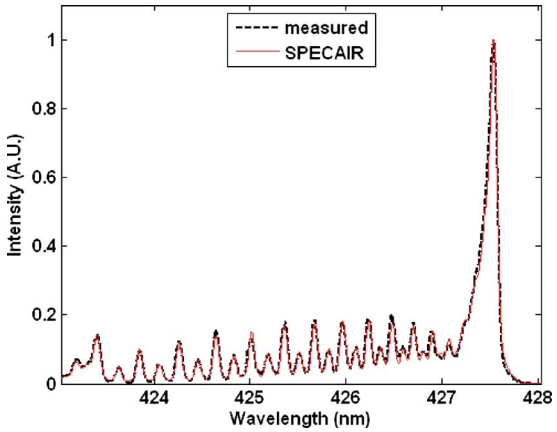

FIG. 10. (Color online) Comparison of the measured high resolution emission spectrum from the N_2^+ first negative system with SPECAIR generated plot for dry air at 760 Torr.

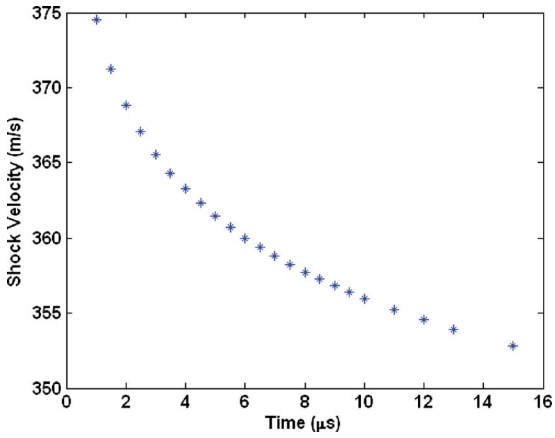

FIG. 11. (Color online) Velocity of the laser induced plasma shockwave in air with STP just ahead of the front.

temperature of 1030 ± 100 K and a vibrational temperature of 1300 ± 100 K. For this experiment, it can be assumed that the molecular translational temperature is equal to the rotational temperature due to the very fast rotational relaxation time at atmospheric pressure.[32]

D. Shockwave velocity and temperature

Using shadowgraph imaging, the velocity of the cylindrical shockwave created by the expanding plasma was measured in air at 760 Torr. The radial position of the shock front was recorded at multiple temporal points starting at $t=1$ μs when the shockwave separated from the plasma and continuing to $t=15$ μs when it left the image area. The laser energy was 260 mJ providing a focused irradiance of 5.5×10^9 W/cm^2. Figure 11 illustrates the velocity of the shockwave that was calculated by taking the numerical derivative of the radial position data. The average velocity of the shockwave was 360 m/s which is slightly larger than the speed of sound in dry air ($\sim$343 m/s) at standard temperature and pressure. Using the tabulated quantities compiled by Zeldovich and Raizer[33] for a shockwave in air with standard pressure and temperature just ahead of the front, the velocity measurements give a gas temperature of approximately 325 K just behind the shockwave front at t=1 μs when it starts to separate from the plasma.

V. SUMMARY

In this work subthreshold breakdown of atmospheric air by a 193 nm excimer laser was experimentally investigated. In addition to the observation of a visible flash in the laser focal region, two-wavelength interferometry measurements also showed substantial electron density (5×10^{16} cm^3) that is not predicted by CC theory at this wavelength and flux. Due to the relatively large photon energy of 6.42 eV at 193 nm, there exists a significant probability of multiphoton ionization processes in air at this wavelength. Using spectroscopic techniques at low pressure where collisional effects are minimized, it was shown that 2+1 REMPI was the rate limiting quantum process for ionization of N_2 to the N_2^+ ($B\,^2\Sigma_u^+$) state. This multiphoton source of electrons seeded the CC process, thereby effectively lowering the threshold

intensity required for breakdown. While it is possible that other multiphoton effects could have also contributed to the seed electron population, it was only N_2^+ that we found direct spectroscopic evidence for in the 300–500 nm wavelength region examined. The REMPI process was determined to enhance the ionization rate so that high density breakdown (5×10^{16} cm^{-3}) at atmospheric conditions could be obtained at a 193 nm, laser radiation flux intensity of 5.5×10^9 W/cm^2, three orders of magnitude below the CC threshold level. The above measurements indicate that the 193 nm subthreshold breakdown plasma will provide an ideal source of seed electrons for long pulse, rf sustained, and larger volume air plasmas.

ACKNOWLEDGMENTS

Research supported by AFOSR Grant No. FA9550-09-1-0357.

[1]N. Kroll and K. Watson, Phys. Rev. A **5**, 1883 (1972).
[2]R. Tambay and R. K. Thareja, J. Appl. Phys. **70**, 2890 (1991).
[3]S. Yalcin, D. R. Crosley, G. P. Smith, and G. W. Faris, Appl. Phys. B: Lasers Opt. **37**, 121 (1998).
[4]S. Soubacq, P. Pignolet, E. Schall, and J. Batina, J. Phys. D **37**, 2686 (2004).
[5]A. D. MacDonald, *Microwave Breakdown in Gases* (Wiley, New York, 1966), pp. 69–120.
[6]P. M. Johnson and C. E. Otis, Annu. Rev. Phys. Chem. **32**, 139 (1981).
[7]H. Mori, T. Ishida, Y. Aoki, and T. Niimi, Rarified Gas Dynamics: 22nd International Symposium, 2001 (unpublished).
[8]L. J. Radziemski and D. A. Cremers, *Laser-Induced Plasmas and Applications* (Dekker, New York, 1989), pp. 1–3.
[9]G. Laufer, A. S. Lee, and H. K. Chelliah, Appl. Opt. **36**, 3278 (1997).
[10]C. Parigger, D. H. Plemmons, J. O. Hornkhol, and J. W. L. Lewis, Appl. Opt. **34**, 3331 (1995).
[11]J. A. Gutherie, X. X. Wang, and L. J. Radziemski, Chem. Phys. Lett. **170**, 117 (1990).
[12]M. Thiyagarajan and J. Scharer, J. Appl. Phys. **104**, 013303 (2008).
[13]M. Thiyagarajan and J. E. Scharer, IEEE Trans. Plasma Sci. **36**, 2512 (2008).
[14]S. Luo, C. M. Denning, and J. E. Scharer, J. Appl. Phys. **104**, 013301 (2008).
[15]G. Bekefi, *Principles of Laser Plasmas* (Wiley, New York, 1976), pp. 457–508.
[16]Y. P. Raizer, *Gas Discharge Physics* (Springer-Verlag, Berlin, 1991), pp. 144–159.
[17]J. Stricker and J. G. Parker, J. Appl. Phys. **53**, 851 (1982).
[18]B. A. Tozer, Phys. Rev. **137**, A1665 (1965).
[19]L. V. Keldysh, Sov. Phys. JETP **20**, 1307 (1965).
[20]R. H. Huddlestone and S. L. Leonard, *Plasma Diagnostic Techniques* (Academic, New York, 1965), pp. 431–433.
[21]B. V. Weber and S. F. Fulghum, Rev. Sci. Instrum. **68**, 1227 (1997).
[22]W. Merzkirch, *Flow Visualization* (Academic, New York, 1974), pp. 111–126.
[23]M. Hipp, J. Woisetschläger, P. Reiterer, and T. Neger, Measurement **36**, 53 (2004).
[24]C. O. Laux, *Radiation and Nonequilibrium Collisional-Radiative Models*, von Karman Institute Lecture Series 2002–07 (Rhode-Saint-Genèse, Belgium, 2002).
[25]S. H. Lin, Y. Fujimura, H. J. Neusser, and E. W. Schlag, *Multiphoton Spectroscopy of Molecules* (Academic, Orlando, 1984), pp. 89–99.
[26]M. Villagran-Muniz, H. Sobral, and R. Novarro-Gonzalez, Meas. Sci. Technol. **14**, 614 (2003).
[27]M. N. Shneider, Z. Zhang, and R. B. Miles, J. Appl. Phys. **104**, 023302 (2008).
[28]G. Baravian, J. Godart, and G. Sultan, Appl. Phys. Lett. **36**, 415 (1980).
[29]K. L. Carleton, K. H. Welge, and S. R. Leone, Chem. Phys. Lett. **115**, 492 (1985).
[30]G. Laufer, R. H. Krauss, and J. H. Grinstead, Opt. Lett. **16**, 1037 (1991).
[31]A. Lofthus and P. H. Krupenie, J. Phys. Chem. Ref. Data **6**, 113 (1977).
[32]C. O. Laux, T. G. Spence, C. H. Kruger, and R. N. Zare, Plasma Sources Sci. Technol. **12**, 125 (2003).
[33]Y. B. Zeldovich and Y. P. Raizer, *Physics of Shock Waves and High-Temperature Hydrodynamic Phenomena* (Academic, New York, 1966), p. 536.